coatings

MDPI

Article

The Tribological Properties of Low-Sulfur and Low-Phosphorus Halogen-Free Ionic Liquids as Lubricants for the Nickel-Based Alloy Inconel 690

Bian Guo [1,*], Mengnan Liu [2], Yan Li [3], Jianming Zheng [3], Xubo Li [1], Chao Peng [3], Zhangshuai Jing [3], Feizhou Li [1] and Qiangliang Yu [4,*]

[1] Shaanxi Key Laboratory of Advanced Manufacturing and Evaluation of Robot Key Components, College of Mechanical Engineering, Baoji University of Arts and Sciences, Baoji 721016, China
[2] State Key Laboratory of Intelligent Agricultural Power Equipment, Luoyang 471039, China
[3] School of Mechanical and Precision Instrument Engineering, Xi'an University of Technology, Xi'an 710048, China; jyxy-ly@xaut.edu.cn (Y.L.)
[4] State Key Laboratory of Solid Lubrication, Lanzhou Institute of Chemical Physics, Chinese Academy of Sciences, Lanzhou 730099, China
* Correspondence: guobian8312@126.com (B.G.); yql@licp.cas.cn (Q.Y.)

Abstract: In this study, we synthesized three low-sulfur and low-phosphorus ionic liquids (ILs). These were $N_{88816}P_8$, $P_{88816}P_8$, and P_{88816}DOSS. The viscosity and thermal stability of the three ILs were analyzed. The tribological properties and lubrication mechanisms of the three ILs were investigated as lubricants for a carbide ball–Inconel 690 nickel-based alloy friction pair and compared at 50 °C and 150 °C. The wear spots of the carbide ball and nickel-based alloy disc samples were characterized using SEM and EDS. The experimental results revealed that $P_{88816}P_8$ had excellent tribological properties. The lubrication mechanism of $P_{88816}P_8$ as a lubricant for the carbide ball–Inconel 690 nickel-based alloy friction pair was investigated using XPS. The excellent friction reduction and anti-wear properties of $P_{88816}P_8$ could be attributed to the tribo-chemistry between $P_{88816}P_8$ and Inconel 690 as well as the formation of a tribo-film on the wear-spot surface. This high-performance IL, suitable for carbide ball–Inconel 690 contact, will be applied to a cutting process of Inconel 690.

Keywords: ionic liquids; Inconel 690; friction reduction and anti-wear; lubrication mechanism; tribo-film

Citation: Guo, B.; Liu, M.; Li, Y.; Zheng, J.; Li, X.; Peng, C.; Jing, Z.; Li, F.; Yu, Q. The Tribological Properties of Low-Sulfur and Low-Phosphorus Halogen-Free Ionic Liquids as Lubricants for the Nickel-Based Alloy Inconel 690. *Coatings* **2023**, *13*, 1793. https://doi.org/10.3390/coatings13101793

Academic Editor: Jurgita Zekonyte

Received: 23 September 2023
Revised: 16 October 2023
Accepted: 17 October 2023
Published: 19 October 2023

1. Introduction

The nickel-based high-temperature alloy Inconel 690 is mainly used as a heat transfer tube material for the steam generators of pressurized water reactor nuclear power plants due to its excellent resistance to intergranular corrosion and intergranular stress corrosion cracking. In our previous work, we observed that cutting fluid had a significant influence on tool life as well as on the surface quality of machined holes during the drilling of holes in nuclear evaporator tube plates [1,2]. Nickel-based high-temperature alloys are difficult to machine due to their low thermal conductivity and high strength [3,4]. Nickel-based high-temperature alloys have the disadvantages of high cutting forces, high temperatures in the cutting area, severe machining hardening, and severe tool wear during the cutting process [5], limiting their wider application. In the cutting process, the lubricant plays an important role in reducing the friction between the tool and the workpiece [6,7]. Lubricants can reduce tool wear, extend the life of the tool, improve the surface quality of the workpiece, and improve the machinability of nickel-based high-temperature alloys [8].

As environmental awareness increases and regulations to protect the ecosystem become more stringent, there is an urgent requirement to develop more environmentally friendly lubricants [9–12]. New opportunities for research in the field of tribology have arisen with the advent of ionic liquids (ILs). ILs are organic molten salts composed only

of anions and cations; they are liquid at or near room temperature [13]. ILs have many excellent properties, including good thermal and chemical stability, low volatility, non-combustibility, and good electrical and thermal conductivity [14,15]. They have a strong boundary adsorption film-forming ability at the friction sub-interface; therefore, they can be used as a high-performance lubricant for cutting processes [16]. These advantages indicate that ILs have the potential to be a promising new class of green lubricants. In recent years, a significant amount of research has been undertaken and researchers in related fields have used ILs as lubricants and lubricant additives [17–20].

Conventional ILs are prone to hydrolysis in humid environments because they contain halogens. This generates hydrogen halides, which are highly corrosive to metal substrate surfaces. The design, preparation, and development of low-sulfur, low-phosphorus, and halogen-free ionic liquids is necessary to reduce corrosion and environmental pollution in the field of tribology [21,22]. Li et al. [23] investigated the ILs P_{888}pDABD and P_{888}pDOSS as lubricants for titanium alloys. They noted that ILs with high contents of sulfur and phosphorus were highly corrosive to metals. Huang et al. [24] studied quaternary ammonium salts and quaternary phosphonium salts in oil-soluble ILs. They observed that they were less corrosive and had excellent tribological properties for steel/steel friction pairs. Yu et al. [25] synthesized the ILs P_{88816}DOSS, P_{888}pDOSS, N_{88816}Sp, and P_{888S}Sp to study their tribological properties and lubrication mechanisms as lubricants for steel–magnesium and steel–aluminum friction pairs. The results revealed that the ILs and the light metals exhibited excellent tribological properties due to the complex tribo-chemistry reaction between them. Fan et al. [26] synthesized and prepared quaternary ammonium ILs with a DOSS anion and used them as lubricants and lubricating additives to investigate the effect of the molecular structure of the ILs on their physicochemical properties and tribological performance. As these ILs were halogen-free, they were non-corrosive and hydrolytically stable to metal substrates; thus, their tribological properties were superior to those of conventional lubricants (e.g., polyalphaolefins). Yu et al. [27] designed and prepared a series of oil-soluble phosphorus-based ILs and used them as candidates for lubrication additives. The research results revealed that their series of ILs had no corrosive effect on either iron or aluminum alloys and demonstrated significant friction reduction and anti-wear properties. Yu et al. [28] designed two oil-soluble ILs—NP-16 and NP-16-2-16, with symmetrical differences in their molecular structure—to perform a series of research works on their anti-corrosion and tribological properties as friction-reducing and anti-wear agents. The corrosion test results revealed that NP-16-2-16 exhibited superior corrosion resistance due to the improved symmetry of its molecular structure. NP-16-2-16 also had a higher maximum snag-free load value (P_B) than NP-16 and had an excellent load-bearing capacity.

The existing research indicates that halogen-free ionic liquids have an active role in reducing corrosion and improving tribological properties. Although researchers have conducted a large number of studies on halogen-free ionic liquids, the focus has mainly been on the friction and lubrication of steel, copper, and aluminum. Research on halogen-free ionic liquids applicable to the friction and lubrication of nickel-based alloys is relatively limited. Therefore, we studied the friction and lubrication characteristics of halogen-free ionic liquids on nickel-based alloys to enable the application of halogen-free ionic liquids in the cutting process of nickel-based alloys.

We synthesized three halogen-free ILs—$N_{88816}P_8$, $P_{88816}P_8$, and P_{88816}DOSS—and systematically studied their physicochemical properties. The three ionic liquids were used as lubricants for a cemented carbide/nickel-based alloy friction pair. The tribological properties of three halogen-free ionic liquids on the nickel-based alloys were systematically investigated using a micromanipulation friction and wear tester. After the tribological tests, the surface morphology of the wear spots was characterized to analyze the wear mechanism. The elemental valence state of the surface of the wear spots as well as the lubrication films were characterized to analyze the lubrication mechanism.

2. Experimental Procedure

2.1. Synthesis of ILs

The raw materials required for the synthesis of the ionic liquids were tri-n-octylamine (purity ≥ 98%), docusate sodium salt (purity ≥ 95%), and tri-n-octylphosphine (purity ≥ 97%). These were purchased from the J&K Scientific Co. and 5/F, Tower A, Junfeng Huating, No. 69 Beichen West Road, Chaoyang District (Beijing, China). The reagents required for the experiments (acetonitrile, anhydrous ethanol, n-hexane, and dichloromethane) were analytically pure. The synthesis and preparation of the three ionic liquids were completed according to the methods reported in the literature [29,30]. Their molecular structures are presented in Figure 1.

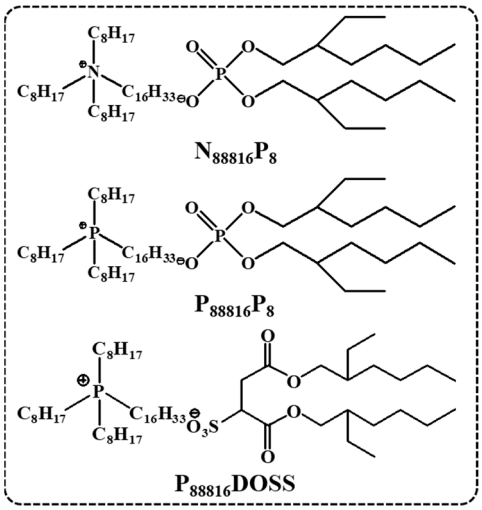

Figure 1. Molecular structures of $N_{88816}P_8$, $P_{88816}P_8$, and $P_{88816}DOSS$.

2.2. Physicochemical Properties

To investigate the viscosity–temperature properties of $N_{88816}P_8$, $P_{88816}P_8$, and $P_{88816}DOSS$, the viscosity of the ILs was measured at 40 °C and 100 °C using an SVM 3000 Stabinger viscometer (Anton Paar, Graz, Austria). The viscosity test was repeated three times and the average value was obtained. After measuring the viscosity of the ILs, the corresponding viscosity was used to calculate the viscosity index (VI) of each specimen according to the international standard ASTM D7042-2012 [2]. The thermal decomposition temperatures of the ILs were analyzed using an STA 449F3 TGA-DSC simultaneous thermal analyzer (Netzsch, Bavaria, Germany). The test method comprised a thermogravimetric (TG) analysis using an alumina crucible under a nitrogen atmosphere. During the TG analysis, the detection temperature was increased from a room temperature of 25 °C to approximately 600 °C at a rate of 10 °C/min. The thermal stability performance of the ILs was evaluated by calculating the percentage of weight lost with the increase in temperature. The thermogravimetric test was repeated twice, and the average value was obtained to improve the reliability of the test.

2.3. Tribological Properties

A friction reduction and anti-wear property test was performed using an SRV-V friction machine (Optimol, Stuttgart, Germany) with a ball–disc mode of contact. The upper specimen comprised a 10 mm diameter carbide ball (YG6x) with a composition of 94.0% tungsten carbide (WC) and 6.0% cobalt (Co) and a hardness of 92.5 HRA. The lower specimen was an Inconel 690 nickel-based alloy disc 24 mm in diameter and 7.9 mm thick. Inconel 690 nickel-based alloy discs have a hardness of 470–480 HV. Prior to the experiment, the surface of the Inconel 690 nickel-based alloy disc was sanded with 800#, 1200#, 1500#, and 2000# SiC sandpaper in turn. The ground surface roughness (Ra) was measured as 0.1μm. The upper-specimen carbide ball (YG6x) moved reciprocally on the surface of the

lower-specimen Inconel 690 nickel-based alloy disc. The friction curve was automatically recorded by a computer throughout the procedure. The tribological test parameters were frequency = 50 Hz, amplitude = 1 mm, and load = 200 N. Each experiment was repeated at least twice.

2.4. Characterization

Following the test, the sample was ultrasonically cleaned with anhydrous ethanol and dried using nitrogen gas. All tests were performed at an ambient relative humidity of 50–54%. A 3D profiler (BRUKER-NPFLEX, Bruker, MA, USA) was used to measure and analyze the wear volume of the lower-specimen steel disc. A microscopic analysis of the wear-spot surface of the upper-specimen ball as well as the lower-specimen Inconel 690 nickel-based alloy disc was performed using a scanning electron microscope (SEM) (FEI Quanta FEG 250, FEI, OR, USA). An elemental analysis of the ground-spot surface of the upper-specimen ball was performed using an X-ray energy spectrometer (EDS) attached to the SEM. XPS was used to analyze and characterize the elemental distribution and valence of the wear spots of the lower-specimen nickel alloy disc as well as to speculate the lubrication mechanism of ILs as lubricants.

3. Results and Discussion

3.1. Viscosity Temperature Performance

Table 1 presents the kinematic viscosity and VI of the $N_{88816}P_8$, $P_{88816}P_8$, and P_{88816}DOSS ILs. From the viscosity test results, we observed that the effect of the cationic differences and anionic differences in the ILs on their viscosity had a certain pattern. $P_{88816}P_8$ had the smallest viscosity at 40 °C; $N_{88816}P_8$ had a slightly larger viscosity than $P_{88816}P_8$. The introduction of N improved the kinematic viscosity of the ILs to an extent. The difference in anions in the ILs had a significant effect on the kinematic viscosity. The kinematic viscosities of P_{88816}DOSS at 40 °C and 100 °C were greater than those of $N_{88816}P_8$ and $P_{88816}P_8$. Structurally, P_{88816}DOSS had a more symmetric molecular structure. This indicated that improving the symmetry of the molecular structure of the ionic liquids was a key factor in improving their kinematic viscosity. Among the three ILs, $P_{88816}P_8$ had the largest VI (169). This implied that $P_{88816}P_8$ was the least affected by temperature. It presented the best viscosity–temperature performance, increasing its suitability as a lubricant.

Table 1. Kinematic viscosity and VI of ILs at 40 °C and 100 °C [2].

IL	Kinematic Viscosity (mm^2/s)		VI
	40 °C	100 °C	
$N_{88816}P_8$	214.2	27.3	163
$P_{88816}P_8$	211.5	27.8	169
P_{88816}DOSS	349.9	38.8	161

3.2. Thermal Stability

The thermal weight loss curves of $N_{88816}P_8$, $P_{88816}P_8$, and P_{88816}DOSS in the range from room temperature to 600 °C are shown in Figure 2. Their corresponding thermal decomposition temperatures are shown in Table 2. From the results of thermal stability analysis, we observed that P_{88816}DOSS had the highest thermal decomposition temperature of 329.15 °C at a 10% weight loss. This was followed by $P_{88816}P_8$ at 314.61 °C. $N_{88816}P_8$ had the lowest thermal decomposition temperature of 209.53 °C at a 10% weight loss when compared with the other two ILs. Due to the cation differences of the ILs, their effect on thermal stability had a certain pattern. Compared with $N_{88816}P_8$, $P_{88816}P_8$ had superior thermal stability. The introduction of P improved the thermal stability of the ILs. The thermal stability performance of P_{88816}DOSS was superior to the other two ILs.

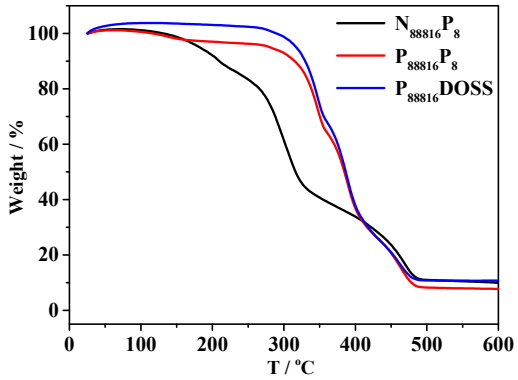

Figure 2. Thermal decomposition curves of ILs.

Table 2. Thermal decomposition temperatures of ILs.

ILs	TG Temperature (°C) Per Weight Loss			
	5%	10%	20%	50%
$N_{88816}P_8$	181.06	209.53	262.07	317.49
$P_{88816}P_8$	275.99	314.61	337.93	384.20
P_{88816}DOSS	316.74	329.15	344.45	387.34

3.3. Tribological Properties

3.3.1. Tribological Properties at 50 °C

Figure 3a reveals the friction coefficient curves of the $N_{88816}P_8$, $P_{88816}P_8$, and P_{88816}DOSS ILs as YG6x–Inconel 690 friction sub-lubricants at 50 °C. The friction coefficients increased and then decreased for all three ILs. $N_{88816}P_8$ had the highest friction coefficient and $P_{88816}P_8$ had the lowest friction coefficient.

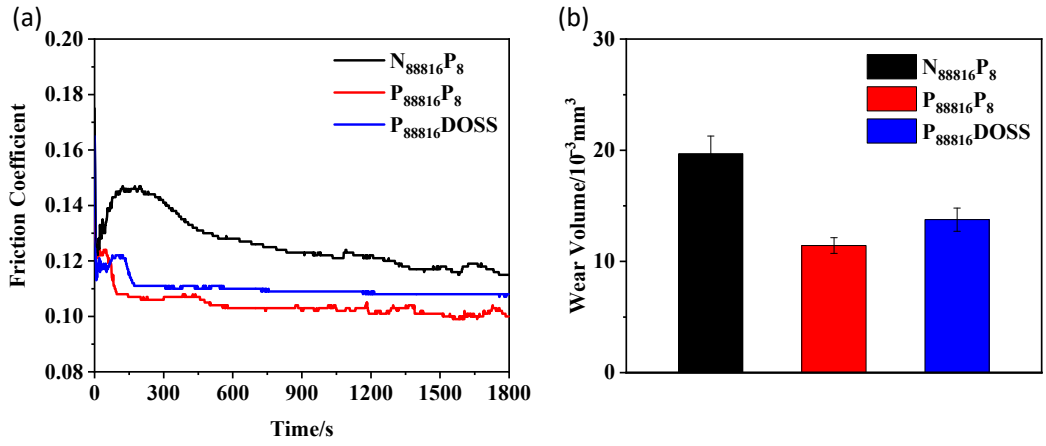

Figure 3. Friction coefficient curves (**a**) and wear volumes (**b**) corresponding with the three ILs at 50 °C.

Figure 3b presents the average wear volumes of the wear spots of the specimen disc with $N_{88816}P_8$, $P_{88816}P_8$, and P_{88816}DOSS as YG6x–Inconel 690 friction sub-lubricants at 50 °C. Figure 4 reveals the 3D profile morphology of the wear spots of the specimen disc with $N_{88816}P_8$, $P_{88816}P_8$, and P_{88816}DOSS as YG6x–Inconel 690 friction sub-lubricants at 50 °C. As seen in Figures 3b and 4, the wear volume of $P_{88816}P_8$ was smaller than that of both $N_{88816}P_8$ and P_{88816}DOSS, indicating that $P_{88816}P_8$ had superior anti-wear performance when compared with $N_{88816}P_8$ and P_{88816}DOSS. These results revealed that $P_{88816}P_8$ had superior friction reduction and anti-wear properties at 50 °C compared with $N_{88816}P_8$ and P_{88816}DOSS.

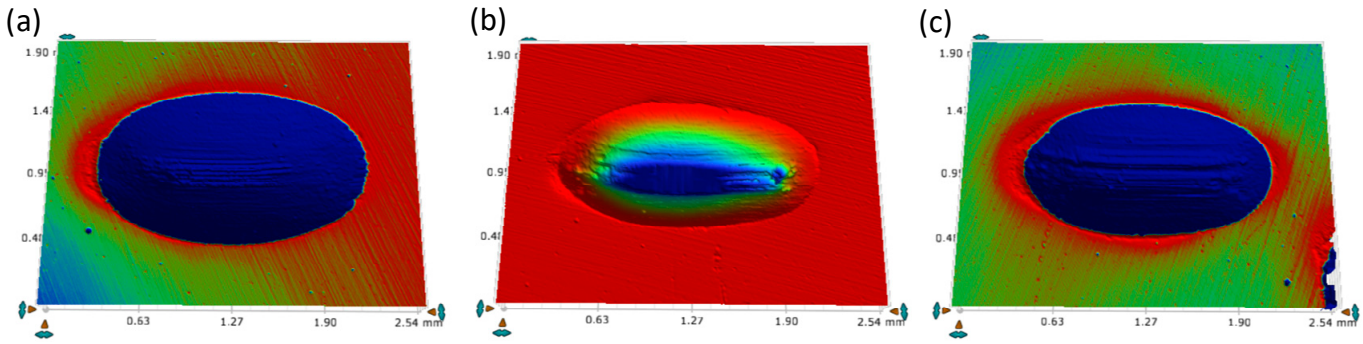

Figure 4. Topographic 3D images of lower sample spots lubricated by ILs at 50 °C: (**a**) $N_{88816}P_8$; (**b**) $P_{88816}P_8$; (**c**) P_{88816}DOSS.

3.3.2. Tribological Properties at 150 °C

Figure 5a presents the friction coefficients of $N_{88816}P_8$, $P_{88816}P_8$, and P_{88816}DOSS as YG6x–Inconel 690 friction sub-lubricants at 150 °C. The friction coefficients increased and then decreased for all three ILs. $P_{88816}P_8$ had a lower coefficient of friction than $N_{88816}P_8$ and P_{88816}DOSS, indicating that $P_{88816}P_8$ had superior friction-reducing properties.

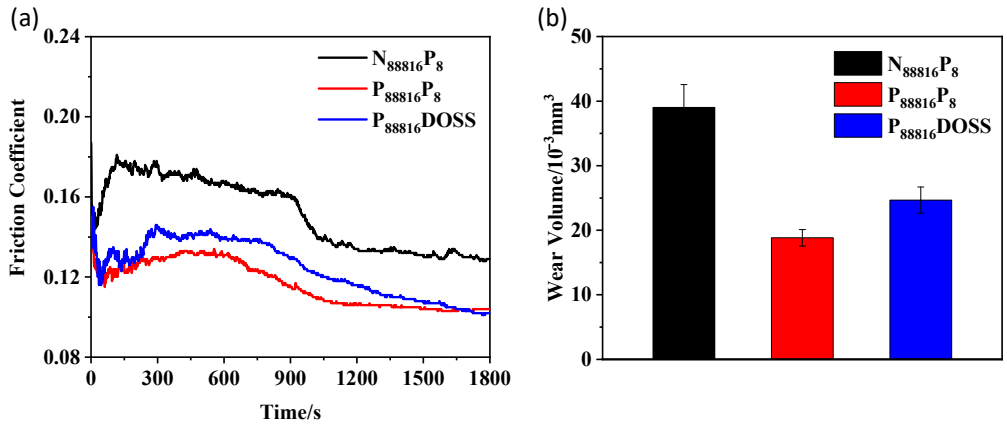

Figure 5. Friction coefficient curves (**a**) and wear volumes (**b**) corresponding with the three ILs at 150 °C.

Figure 5b reveals the average wear volumes of the wear spots of the specimen disc with $N_{88816}P_8$, $P_{88816}P_8$, and P_{88816}DOSS as YG6x–Inconel 690 friction sub-lubricants at 150 °C. Figure 6 depicts the 3D contours of the wear spots of the specimen disc with $N_{88816}P_8$, $P_{88816}P_8$, and P_{88816}DOSS as YG6x–Inconel 690 friction sub-lubricants at 150 °C. As seen in Figures 5b and 6, the wear volume loss of $P_{88816}P_8$ was less than that of the other two ILs, indicating that $P_{88816}P_8$ had superior anti-wear performance.

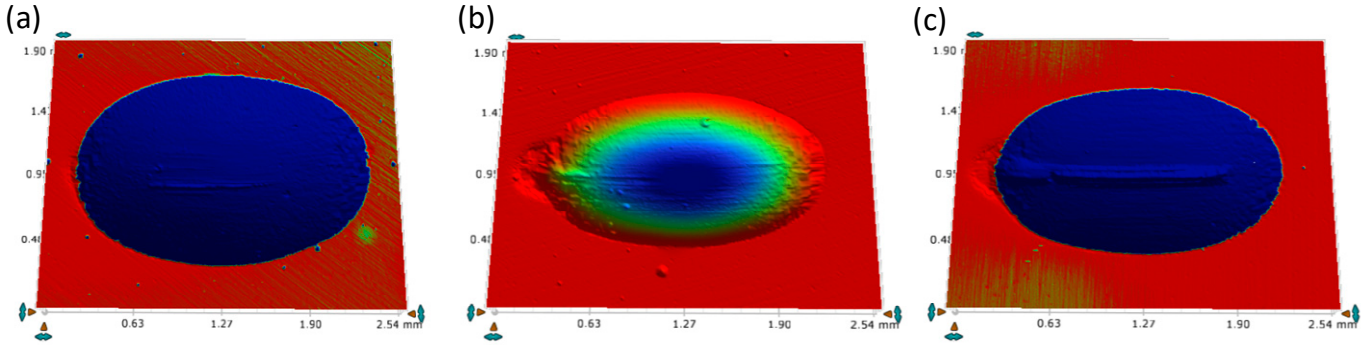

Figure 6. Topographic 3D images of lower sample spots lubricated by ILs at 150 °C: (**a**) $N_{88816}P_8$; (**b**) $P_{88816}P_8$; (**c**) P_{88816}DOSS.

The primary reason for the excellent anti-friction and anti-wear performance of $P_{88816}P_8$ was because the anionic phosphate ester in $P_{88816}P_8$ was adsorbed on the friction surface. Under the action of friction heat, physical adsorption and friction chemical reactions occur [20]. A lubricating film is generated on the friction surface to prevent direct contact between cemented carbide and nickel-based alloys [15,31,32]. The lubricating film plays a role in reducing friction, promoting anti-wear.

3.3.3. Effect of Load on the Tribological Properties

We investigated the extreme pressure performance of the IL lubricants in depth by varying the load. The results are presented in Figure 7. The test load used was from 200 N to approximately 2000 N, increasing by 100 N/2 min. The friction coefficient of $N_{88816}P_8$ tended to increase with an increase in load at 50 °C and the friction coefficient was larger. The friction coefficients of both $N_{88816}P_8$ and P_{88816}DOSS were lower and relatively smoother. As seen in Figure 7b, the friction coefficient of $N_{88816}P_8$ was the largest with an increase in load at 150 °C, revealing a trend of increasing and then decreasing. The friction coefficients of $P_{88816}P_8$ and P_{88816}DOSS were smaller and tended to increase, but not significantly. $N_{88816}P_8$ had a higher friction coefficient, whereas both $N_{88816}P_8$ and P_{88816}DOSS had lower friction coefficients and were relatively smooth. $N_{88816}P_8$ and P_{88816}DOSS had excellent extreme pressure properties and tended to form stronger tribo-films with the metal substrate surfaces [23]. The specific composition and the specific type of tribo-films formed require further investigation.

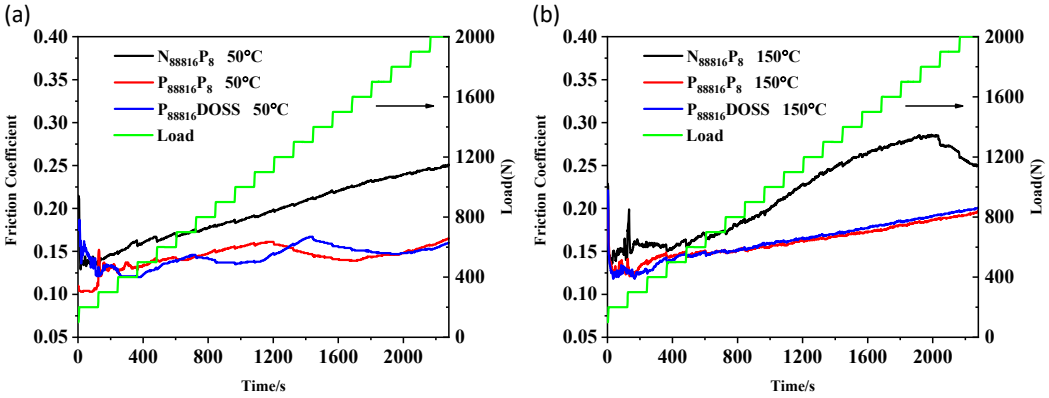

Figure 7. Curves of friction coefficient vs. time during a load slope test from 200 N to 2000 N when lubricated by different ionic liquids at (**a**) 50 °C and (**b**) 150 °C.

3.3.4. Effect of Temperature on the Tribological Properties

To evaluate the effect of temperature on the friction performance, we conducted a variable temperature test with the ILs. The friction coefficients of $N_{88816}P_8$, $P_{88816}P_8$, and P_{88816}DOSS were tested at a rate of 25 °C with a rise every 4 min from 50 °C to approximately 350 °C under a load of 200 N, as shown in Figure 8. The friction coefficient of $N_{88816}P_8$ first decreased and then increased to the maximum value. The friction coefficients of $P_{88816}P_8$ and P_{88816}DOSS increased and then decreased. $P_{88816}P_8$ had the lowest friction coefficient.

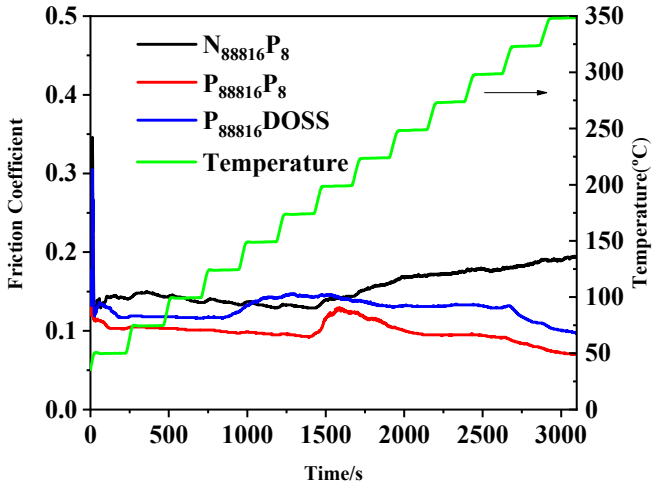

Figure 8. Curves of friction coefficient vs. time during a temperature slope test from 50 °C to 350 °C when lubricated by different ionic liquids.

3.4. Characterization

Figure 9 presents the SEM images of the lower-specimen Inconel 690 nickel-based alloy wear spots. The SEM images of $N_{88816}P_8$ obtained at 50 °C (Figure 9a) and 150 °C (Figure 9d) clearly revealed that the wear was more severe at high temperatures and the resulting wear spots were larger. At 50 °C, a clear furrow could be seen on the lower specimen (Figure 9a1). Under high-temperature conditions, the furrow almost disappeared and the resulting friction surface was smooth (Figure 9d1). Significant adhesive wear could be observed in the wear spots at both low and high temperatures (Figure 9a1,d1). The SEM images obtained for $P_{88816}P_8$ at 50 °C (Figure 9b) and 150 °C (Figure 9e) clearly revealed that these wear spots were the smallest. The grinding spots obtained at a high temperature (Figure 9e) were larger than those obtained at a low temperature. At 50 °C, a clear furrow could be seen on the surface of the lower specimen (Figure 9b1). Under high-temperature conditions, the surface quality of the lower specimen was significantly enhanced (Figure 9e1). Whether at 50 °C or 150 °C, $P_{88816}P_8$ exhibited an excellent anti-wear action. In contrast, the SEM images obtained for P_{88816}DOSS at both 50 °C (Figure 9c) and 150 °C (Figure 9f) clearly revealed a medium surface size of the wear spots and that adhesive wear occurred on the wear spots.

Figure 10 presents the SEM images of the surface wear spots on the worn carbide ball of the upper specimen. The SEM images of $N_{88816}P_8$ obtained at 50 °C (Figure 10a) and 150 °C (Figure 10d) clearly revealed that the wear spots were deeper. The wear under high-temperature conditions was more severe and the wear spots were larger. At 50 °C, a clear furrow could be seen in the wear spots of the upper-specimen ball (Figure 10a1). Under high-temperature conditions, there were almost no furrows and the resulting friction surface was smooth (Figure 10d1). The SEM images obtained for $P_{88816}P_8$ at 50 °C (Figure 10b) and 150 °C (Figure 10e) clearly revealed that both wear spots were shallower. The adhesive wear was more severe under high-temperature conditions, and the obtained wear spots were larger (Figure 10e), with obvious ploughing and adhesive wear on the surface of the wear spots. The SEM images obtained for P_{88816}DOSS at both 50 °C (Figure 10c) and 150 °C (Figure 10f) clearly revealed that the wear spots were deeper and of medium size, with corrosion wear occurring on the spot at 50 °C (Figure 10c1) and deep pits on the spot at 150 °C.

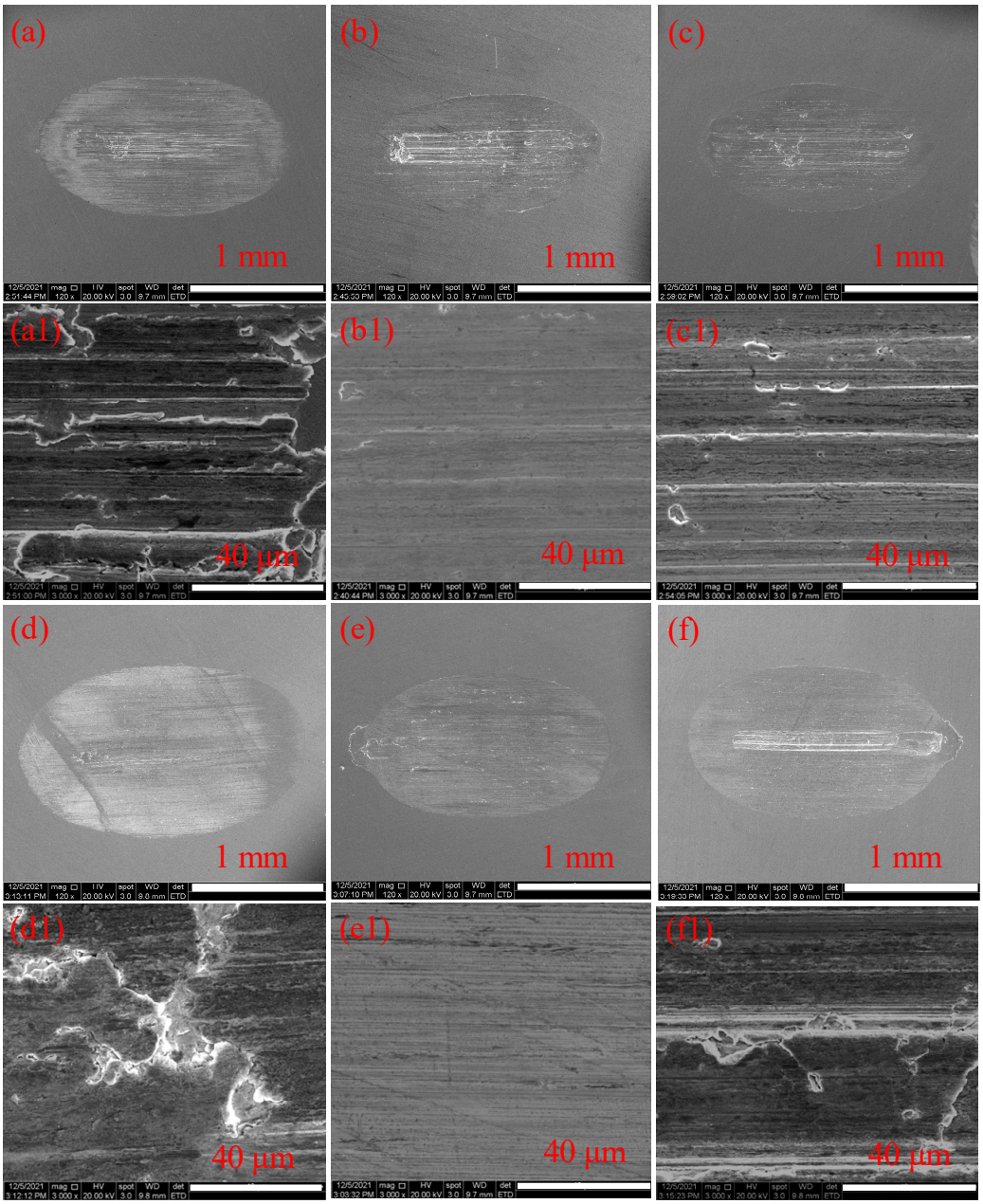

Figure 9. SEM micrographs of the worn surfaces of the lower specimen lubricated by different ionic liquids: (**a**) $N_{88816}P_8$, 50 °C; (**b**) $P_{88816}P_8$, 50 °C; (**c**) P_{88816}DOSS, 50 °C; (**a1**) $N_{88816}P_8$, 50 °C; (**b1**) $P_{88816}P_8$, 50 °C; (**c1**) P_{88816}DOSS, 50 °C; (**d**) $N_{88816}P_8$, 150 °C; (**e**) $P_{88816}P_8$, 150 °C; (**f**) P_{88816}DOSS, 150 °C; (**d1**) $N_{88816}P_8$, 150 °C; (**e1**) $P_{88816}P_8$, 150 °C; (**f1**) P_{88816}DOSS, 150 °C.

Figure 11 presents the EDS of the upper-specimen carbide ball lubricated by the three ILs at 50 °C and 150 °C. The wear spots of the upper-specimen carbide ball at 50 °C had obvious furrows and serious adhesive wear. The furrows were barely visible at 150 °C, and there were a few areas with pits caused by adhesive wear. As can be seen in Figure 11a1, the presence of Ni, O, and P in the wear spots of the carbide ball at 150 °C indicated the involvement of these elements in the tribo-chemical reaction. P and O may be responsible for the formation of brittle phases, which lead to adhesive wear and abrasive grain wear.

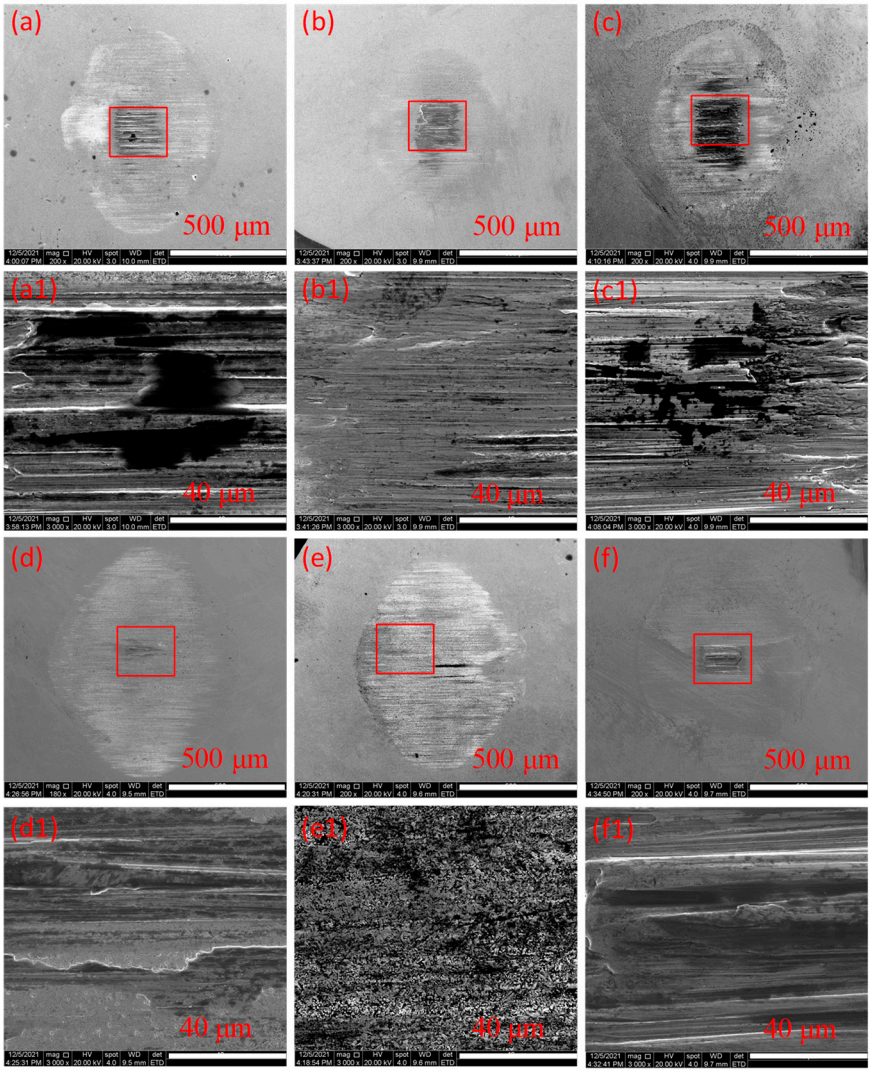

Figure 10. SEM micrographs of the worn surfaces of the upper-specimen ball lubricated by different ionic liquids: (**a**) $N_{88816}P_8$, 50 °C; (**b**) $P_{88816}P_8$, 50 °C; (**c**) P_{88816}DOSS, 50 °C; (**a1**) $N_{88816}P_8$, 50 °C; (**b1**) $P_{88816}P_8$, 50 °C; (**c1**) P_{88816}DOSS, 50 °C; (**d**) $N_{88816}P_8$, 150 °C; (**e**) $P_{88816}P_8$, 150 °C; (**f**) P_{88816}DOSS, 150 °C; (**d1**) $N_{88816}P_8$, 150 °C; (**e1**) $P_{88816}P_8$, 150 °C; (**f1**) P_{88816}DOSS, 150 °C.

Figure 11b depicts the wear spots of the $P_{88816}P_8$-lubricated upper-specimen carbide ball at 50 °C. Adhesive wear occurred, as further evidenced by the increased content of nickel elements in the EDS. Several elements of the Inconel 690 disc were transferred to the upper-specimen carbide-ball interface. Figure 11b1 depicts the $P_{88816}P_8$-lubricated upper-specimen carbide ball at 150 °C. As seen in Figure 11b1, the Ni content on the surface of the ball was low, indicating that the surface of the friction sub-surface did not experience severe adhesive wear and the surface quality was good. Figure 11c depicts the wear spot of the $P_{88816}P_8$-lubricated upper-specimen carbide ball at 50 °C. More severe adhesive wear occurred and certain elements of the Inconel 690 disc were transferred to the carbide ball of the upper specimen. Figure 11c1 depicts the $P_{88816}P_8$-lubricated upper-specimen carbide ball at 150 °C. There were fewer Ni elements at the carbide-ball interface, indicating that the adhesive wear that occurred at the friction sub-interface was lighter. However, the wear marks were deeper.

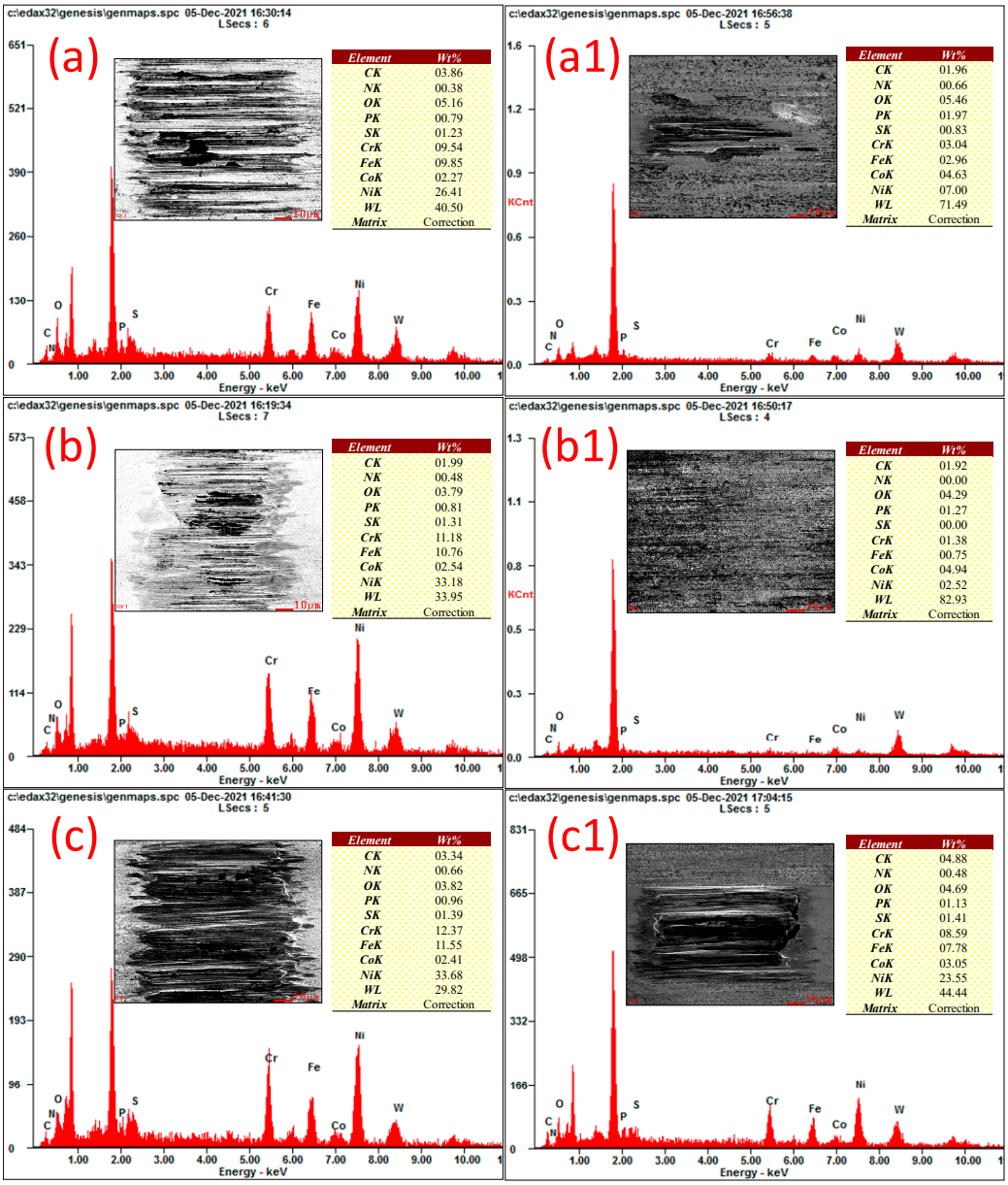

Figure 11. EDS of the worn surfaces of the upper-specimen ball lubricated by different ionic liquids: (**a**) $N_{88816}P_8$, 50 °C; (**a1**) $N_{88816}P_8$, 150 °C; (**b**) $P_{88816}P_8$, 50 °C; (**b1**) $P_{88816}P_8$, 150 °C; (**c**) P_{88816}DOSS, 50 °C; (**c1**) P_{88816}DOSS, 150 °C.

3.5. XPS

To obtain a deeper understanding of the lubrication mechanism of $N_{88816}P_8$, $P_{88816}P_8$, and P_{88816}DOSS on the surface of the nickel-based high-temperature alloy Inconel 690, the chemical composition of the wear-spot surfaces lubricated by ILs at 50 °C and 150 °C was analyzed using XPS.

Figures 12 and 13 present the spectra of C1s, O1s, Ni2p, N1s, S2p, and P2p of the specimen grinding spots at 50 °C and 150 °C, respectively. The shape and binding energy of each element were basically similar [33,34]. Consequently, when ILs were used as lubricants, the tribo-chemical reaction process was approximately the same [35]. The peak of the binding energy appeared at 284.8 eV, corresponding with C-C [36]. The absorption peak of P2p appeared near 133.2 eV. Combined with the absorption peaks of O1s at 856.2 eV and Ni2p near 861.3 eV, we inferred that $NiPO_4$ was generated at the wear interface [37–39].

The combined absorption peaks of Ni2p, O1s, and S2p near 169.9 eV indicated the formation of $NiSO_4$ at the wear interface [25,40].

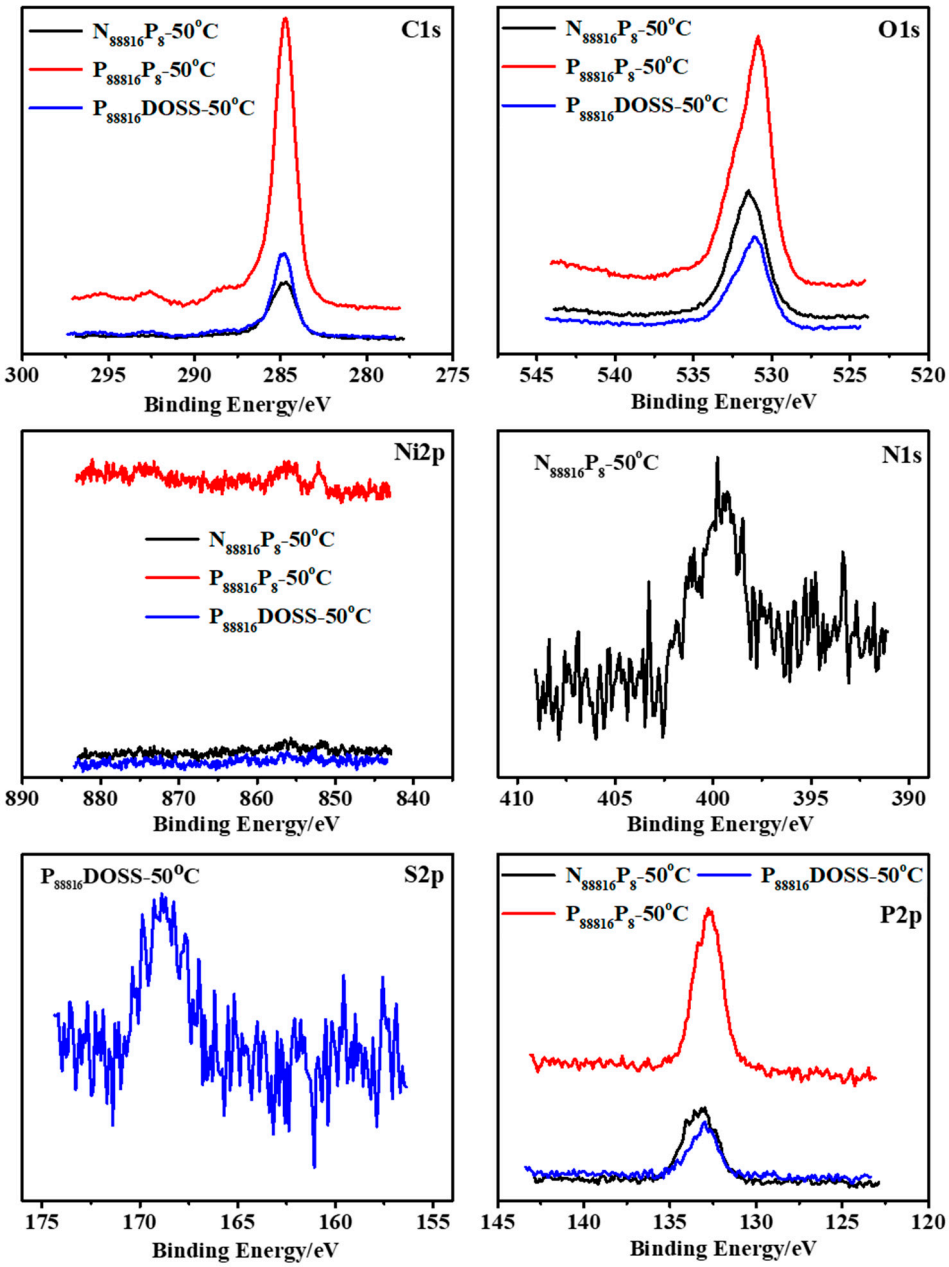

Figure 12. XPS precision spectra of each element after lubrication using $N_{88816}P_8$, $P_{88816}P_8$, and P_{88816}DOSS at 50 °C.

The above results revealed that $P_{88816}P_8$ had superior anti-wear performance. The primary reason was due to the active element of P in $P_{88816}P_8$ and Ni, Cr, and Fe in the Inconel 690 nickel-based alloy disc of the lower specimen. Under the action of frictional heat, physical adsorption and tribo-chemical reactions occurred, resulting in inorganic compounds with high toughness (such as nickel phosphate) which, in turn, formed a tribo-film on the friction surface to prevent direct contact between the tungsten carbide and Inconel 690. This lubricating protective film played a role in reducing the friction coefficient. At high temperatures, the ILs were more likely to have tribo-chemical reactions with the friction pair. $P_{88816}P_8$ generated a thicker tribo-film; thus, it was more suitable for the lubrication of nickel-based high-temperature alloys.

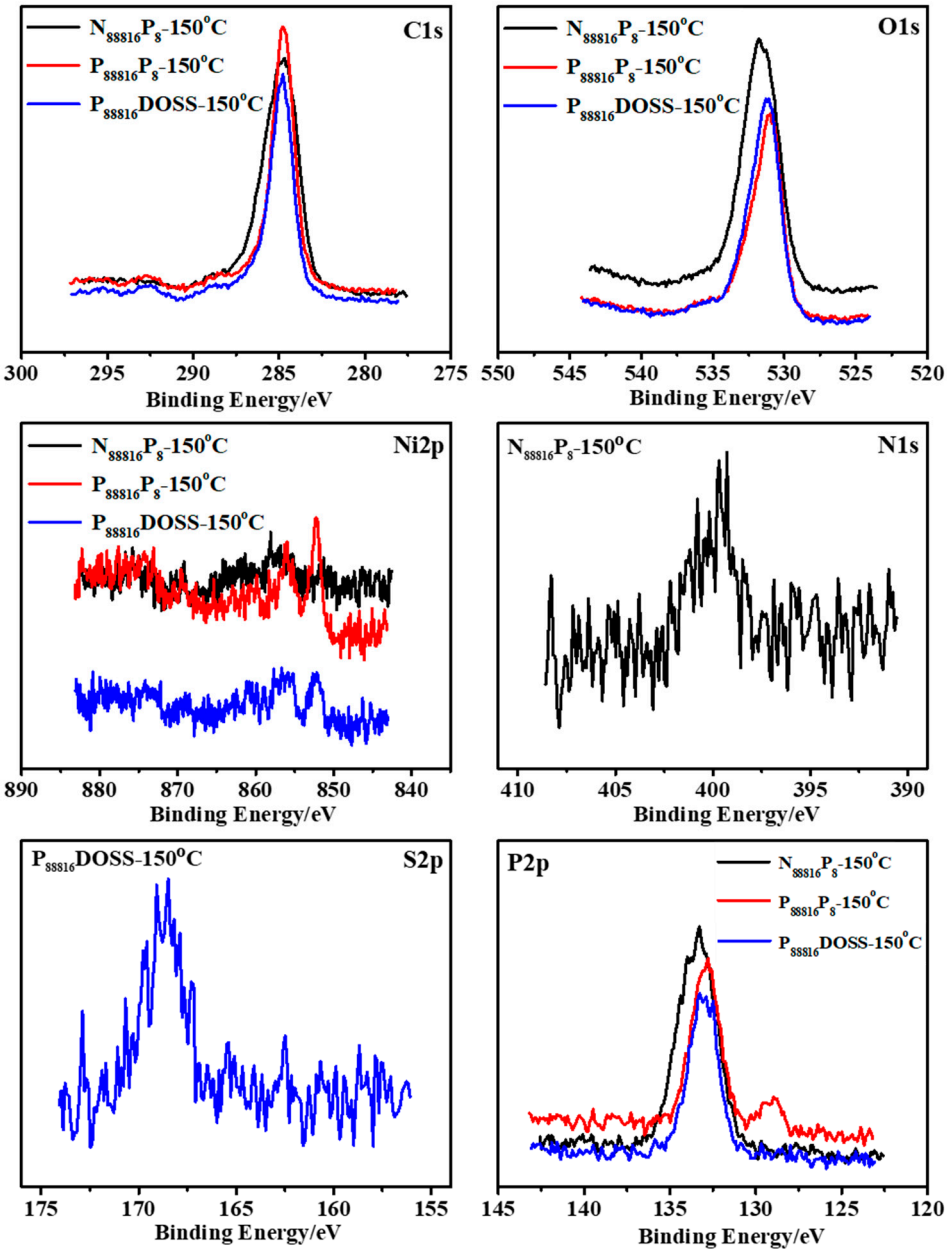

Figure 13. XPS precision spectra of each element after lubrication using $N_{88816}P_8$, $P_{88816}P_8$, and P_{88816}DOSS at 150 °C.

4. Conclusions

We synthesized three low-sulfur and low-phosphorus ILs. These were $N_{88816}P_8$, $P_{88816}P_8$, and P_{88816}DOSS. The viscosity and thermal stability of the three ILs were analyzed. The results revealed that the kinematic viscosity of the ionic liquid P_{88816}DOSS was greater than that of $N_{88816}P_8$ and $P_{88816}P_8$. $P_{88816}P_8$ had the largest viscosity index, as well as excellent viscosity–temperature properties and thermal stability.

The tribological properties of the three ILs as lubricants for a carbide ball–Inconel 690 nickel-based alloy friction pair were investigated at 50 °C and 150 °C. The experimental results revealed that the coefficient of friction and wear volume of $P_{88816}P_8$ were smaller than those of P_{88816}DOSS and $N_{88816}P_8$. $P_{88816}P_8$ had excellent tribological properties.

The lubrication mechanism of $P_{88816}P_8$ was investigated using XPS. The excellent friction reduction and anti-wear properties of $P_{88816}P_8$ could be attributed to the tribochemical reaction between the active element P in $P_{88816}P_8$ and Ni, Cr, and Fe in the Inconel

690 nickel-based alloy, along with the formation of a tribo-film of inorganic compounds with high toughness (e.g., nickel phosphate) on the wear-spot surface. This lubricating film prevented direct contact between the carbide and the nickel-based alloy. This high-performance IL, suitable for carbide ball–Inconel 690 contact, will be applied to a cutting process of Inconel 690.

Author Contributions: Conceptualization, B.G., Y.L. and Q.Y.; methodology, B.G. and J.Z.; software, X.L.; validation, C.P., Z.J. and F.L.; formal analysis, X.L.; data curation, B.G., C.P. and Z.J.; writing—original draft preparation, B.G. and Y.L.; writing—review and editing, J.Z. and Q.Y.; supervision, Q.Y.; funding acquisition, B.G. and M.L. All authors have read and agreed to the published version of the manuscript.

Funding: This research was funded by the National Natural Science Foundation of China, grant number 52075524; the Open Project of State Key Laboratory of Intelligent Agricultural Power Equipment, grant number SKT2022003; the Natural Science Basic Research Program of Shaanxi Province of China, grant number 2023-JC-QN-0571; and the Service Local Special Scientific Research Program Project of Shaanxi Provincial Department of Education, grant number 23JC002.

Institutional Review Board Statement: Not applicable.

Informed Consent Statement: Not applicable.

Data Availability Statement: Not applicable.

Acknowledgments: The authors are grateful to the National Natural Science Foundation of China, the Open Project of State Key Laboratory of Intelligent Agricultural Power Equipment, the Natural Science Basic Research Program of Shaanxi Province of China, and the Service Local Special Scientific Research Program Project of Shaanxi Provincial Department of Education.

Conflicts of Interest: The authors declare no conflict of interest.

References

1. Li, X.; Zheng, J.; Li, Y.; Xiao, J.; Guo, B.; Liu, C. Modeling and experimental investigation of drilling force for low-frequency axial vibration-assisted BTA deep hole drilling. *J. Adv. Manuf. Technol.* **2020**, *111*, 1721–1733. [CrossRef]
2. Guo, B.; Li, Y.; Zheng, J.; Li, F.; Li, X.; Du, X.; Yuan, L. Tribological properties of a halogen-free ionic liquid for Inconel 690–tungsten carbide contact. *Tribol. Int.* **2021**, *163*, 107153. [CrossRef]
3. Anwar, S.; Khan, N.; Khan, S.; Raza, S. One-Step High-Speed Finish Drilling of Inconel 718 Superalloy via Novel Inserts. *Processes* **2023**, *11*, 752. [CrossRef]
4. Ceritbinmez, F.; Günen, A.; Gürol, U.; Çam, G. A comparative study on drillability of Inconel 625 alloy fabricated by wire arc additive manufacturing. *J. Manuf. Process.* **2023**, *89*, 150–169. [CrossRef]
5. Naresh Babu, M.; Anandan, V.; Dinesh Babu, M. Performance of ionic liquid as a lubricant in turning inconel 825 via minimum quantity lubrication method. *J. Manuf. Process.* **2021**, *64*, 793–804. [CrossRef]
6. Mousavi, S.; Heris, S. Experimental investigation of ZnO nanoparticles effects on thermophysical and tribological properties of diesel oil. *Int. J. Hydrogen Energy* **2020**, *45*, 23603–23614. [CrossRef]
7. Mousavi, S.; Heris, S.; Hosseini, M. Experimental investigation of MoS_2/diesel oil nanofluid thermophysical and rheological properties. *Int. Commun. Heat Mass Transf.* **2019**, *108*, 104298. [CrossRef]
8. Szwajka, K.; Zielinska-Szwajka, J.; Zaba, K.; Trzepiecinski, T. An Investigation of the Sequential Micro-Laser Drilling and Conventional Re-Drilling of Angled Holes in an Inconel 625 Ni-Based Alloy. *Lubricants* **2023**, *11*, 384. [CrossRef]
9. Tang, Q.; Zhao, Z.; Li, T.; Ge, L.; Xu, H.; Liu, L.; Dong, J. Methyl oleate-alkylated tetralin with dual-functional groups as base oil with PAO to improve the performance of lithium-based grease. *Tribol. Lett.* **2023**, *71*, 104. [CrossRef]
10. Wang, R.; Sun, C.; Yan, X.; Guo, T.; Xiang, W.; Yang, Z.; Yu, Q.; Yu, B.; Cai, M.; Zhou, F. Influence of the molecular structure on the tribological properties of choline-based ionic liquids as water-based additives under current-carrying lubrication. *J. Mol. Struct.* **2023**, *369*, 120868. [CrossRef]
11. Guo, H.; Stoyanovich, B.; Pang, J.; Iglesias, P. Lubricating Ability of Protic Ionic Liquids as Additives to a Biodegradable Oil for Aluminum-Steel Contact: Effect of Alkyl Chain Length and Propensity to Hydrogen Bonding. *Lubricants* **2023**, *11*, 329. [CrossRef]
12. Ahmadi, N.; Rezazadeh, S. An Innovative Approach to Predict the Diffusion Rate of Reactant's Effects on the Performance of the Polymer Electrolyte Membrane Fuel Cell. *Mathematics* **2023**, *11*, 4094. [CrossRef]
13. Gulzar, M.; Masjuki, H.H.; Kalam, M.A.; Varman, M.; Zulkifli, N.W.M.; Mufti, R.A.; Rehan, Z. Tribological performance of nanoparticles as lubricating oil additives. *J. Nanopart. Res.* **2016**, *18*, 223. [CrossRef]
14. Ye, C.; Liu, W.; Chen, Y.; Yu, L. Room-temperature ionic liquids: A novel versatile lubricant. *Chem. Commun.* **2001**, *21*, 2244–2245. [CrossRef] [PubMed]

15. Zhou, F.; Liang, Y.; Liu, W. Ionic liquid lubricants: Designed chemistry for engineering applications. *Chem. Soc. Rev.* **2009**, *38*, 2590–2599. [CrossRef]
16. Zhao, J.; Huang, Y.; He, Y.; Shi, Y. Nanolubricant additives: A review. *Friction* **2021**, *9*, 891–917. [CrossRef]
17. Fan, Z.; Xiang, Z.; Tang, B.; Chen, W.; Qian, H.; Mo, J.; Zhou, Z. Effect of surface modification on the tribological properties of friction blocks in high-speed train brake systems. *Tribol. Lett.* **2021**, *69*, 27. [CrossRef]
18. González, R.; Viesca, J.L.; Hernández Battez, A.; Hadfield, M.; Fernández-González, A.; Bartolomé, M. Two phosphonium cation-based ionic liquids as lubricant additive to a polyalphaolefin base oil. *J. Mol. Liq.* **2019**, *293*, 111536. [CrossRef]
19. Goindi, G.S.; Sarkar, P.; Jayal, A.D.; Chavan, S.N.; Mandal, D. Investigation of ionic liquids as additives to canola oil in minimum quantity lubrication milling of plain medium carbon steel. *Int. J. Adv. Manuf. Technol.* **2018**, *94*, 881–896. [CrossRef]
20. Cai, M.; Yu, Q.; Zhou, F.; Liu, W. Physicochemistry aspects on frictional interfaces. *Friction* **2017**, *5*, 361–382. [CrossRef]
21. Roy, S.; Speed, L., Jr.; Viola, M.; Luo, H.; Leonard, D.; Qu, J. Oil miscible phosphonium-phosphate ionic liquid as novel antiwear and antipitting additive for low-viscosity rear axle lubricants. *Wear* **2021**, *466*, 203588. [CrossRef]
22. Yang, S.; Zhang, D.; Wong, J.; Cai, M. Interactions between ZDDP and an oil-soluble ionic liquid additive. *Tribol. Int.* **2021**, *158*, 106938. [CrossRef]
23. Li, F.; Guo, B. Effect of different lubricants on microstructural and tribological properties of TC21 titanium alloy against Si3N4 under fretting–reciprocating sliding. *J. Alloys Compd.* **2018**, *743*, 576–585. [CrossRef]
24. Huang, G.; Yu, Q.; Ma, Z.; Cai, M.; Zhou, F.; Liu, W. Oil-soluble ionic liquids as antiwear and extreme pressure additives in poly-α-olefin for steel/steel contacts. *Friction* **2019**, *7*, 18–31. [CrossRef]
25. Yu, Q.; Zhang, C.; Dong, R.; Shi, Y.; Wang, Y.; Bai, Y.; Zhang, J.; Cai, M.; Zhou, F.; Liu, W. Physicochemical and tribological properties of gemini-type halogen-free dicationic ionic liquids. *Friction* **2021**, *9*, 344–355. [CrossRef]
26. Fan, M.; Yang, D.; Wang, X.; Liu, W.; Fu, H. Doss–based QAILs: As both neat lubricants and lubricant additives with excellent tribological properties and good detergency. *Ind. Eng. Chem. Res.* **2014**, *53*, 17952–17960. [CrossRef]
27. Yu, B.; Bansal, D.G.; Qu, J.; Sun, X.; Luo, H.; Dai, S.; Blau, P.J.; Bunting, B.G.; Mordukhovich, G.; Smolenski, D.J. Oil-miscible and non-corrosive phosphonium-based ionic liquids as candidate lubricant additives. *Wear* **2012**, *289*, 58–64. [CrossRef]
28. Yu, Q.; Zhang, C.; Dong, R.; Shi, Y.; Wang, Y.; Bai, Y.; Zhang, J.; Cai, M.; Zhou, F.; Novel, N. P-containing oil-soluble ionic liquids with excellent tribological and anti-corrosion performance. *Tribol. Int.* **2019**, *132*, 118–129. [CrossRef]
29. Yang, Z.; Liang, Y.; Huang, Q.; Wang, X.; Zhou, C.; Wang, R.; Yan, X.; Yu, B.; Yu, Q.; Cai, M.; et al. Tribological performance study of oil-soluble ILs as lubricant additives by the four-ball method. *Lubr. Sci.* **2022**, *35*, 183–192. [CrossRef]
30. Li, F.; Yang, Z.; Guo, B.; Liang, Y.; Zhou, K.; Lv, H.; Feng, F.; Huang, Q.; Yu, Q.; Cai, M.; et al. Tribological performance of two oil-soluble ionic liquids compared with imported additives. *Surf. Technol.* **2022**, *52*, 1–23. [CrossRef]
31. Günen, A.; Ergin, Ö. A Comparative Study on Characterization and High-Temperature Wear Behaviors of Thermochemical Coatings Applied to Cobalt-Based Haynes 25 Superalloys. *Coatings* **2023**, *13*, 1272. [CrossRef]
32. Feng, K.; Shao, T. The evolution mechanism of tribo-oxide layer during high temperature dry sliding wear for nickel-based superalloy. *Wear* **2021**, *476*, 203747. [CrossRef]
33. Chen, W.; Wang, K.; Gao, Y.; He, N.; Xin, H.; Li, H. Investigation of tribological properties of silicon nitride ceramic composites sliding against titanium alloy under artificial seawater lubricating condition. *Int. J. Refract. Met. Hard Mater.* **2018**, *76*, 204–213. [CrossRef]
34. Wang, Z.; Chang, J.; Cai, C. Tribological performance of phosphonium ionic liquids as additives in lithium lubricating grease. *Lubricants* **2018**, *6*, 23. [CrossRef]
35. Cui, S.; Zhu, H.; Tieu, A.K.; Deng, G.; Wan, S.; Zhu, Q.; Lin, B. Insights into the behavior of polyphosphate lubricant in hot rolling of mild steel. *Wear* **2019**, *426*, 433–442. [CrossRef]
36. Li, X.; Deng, S.; Du, G.; Xie, X. Synergistic inhibition effect of walnut green husk extract and sodium lignosulfonate on the corrosion of cold rolled steel in phosphoric acid solution. *J. Taiwan Inst. Chem. Eng.* **2020**, *114*, 263–283. [CrossRef]
37. Su, F.; Chen, G.; Huang, P. Lubricating performances of graphene oxide and onion-like carbon as water-based lubricant additives for smooth and sand-blasted steel discs. *Friction* **2020**, *8*, 47–57. [CrossRef]
38. Fan, M.; Jin, Y.; Han, Y.; Ma, L.; Li, W.; Lu, Y.; Zhou, F.; Liu, W. The effect of chemical structure on the tribological performance of perfluorosulfonate ILs as lubricants for Ti-6Al-4V tribopairs. *J. Mol. Liq.* **2021**, *321*, 114286. [CrossRef]
39. Li, S.; Chen, H.; Luo, T.; Wang, F.; Xiao, G.; Chen, Z.; Yi, M.; Sheng, C.; Xu, C. Tribological properties of 1-octyl-3-methylimidazolium lactate ionic liquid as a lubricant additive. *J. Mol. Liq.* **2021**, *332*, 115828. [CrossRef]
40. Wu, J.; Luo, Y.; Chen, Y.; Lu, X.; Feng, X.; Bao, N.; Shi, Y. Poly (ionic liquid) s as lubricant additives with insight into adsorption-lubrication relationship. *Tribol. Int.* **2022**, *165*, 107278. [CrossRef]